Performance of the dynamic single photon emission computed tomography (dSPECT) method for decreasing or increasing activity changes

A Celler†‡¶, T Farncombe‡, C Bever‡, D Noll§, J Maeght§, R Harrop†‖ and D Lyster†‡

† Vancouver Hospital and Health Sciences Centre, Vancouver, Canada
‡ University of British Columbia, Vancouver, Canada
§ Laboratoire MIP, Université Paul Sabatier, Toulouse, France
‖ Simon Fraser University, Burnaby, Canada

E-mail: `aceller@physics.ubc.ca`

Abstract. Radionuclide imaging is now widely used whenever functional information is required. We present a new approach to dynamic SPECT imaging (dSPECT method) that uses a single slow rotation of a conventional camera and allows us to reconstruct a series of 3D images corresponding to the radiotracer distribution in the body at various times. Using simulations of various camera configurations and acquisition protocols, we have shown that this method is able to reconstruct washout half-lives with an accuracy greater than 90% when used with triple-head SPECT cameras. Accuracy decreases when using fewer camera heads, but dual-head geometries still give an accuracy greater than 80% for short and 90% for long half-lives and about 50–75% for single-head systems. Dynamic phantom experiments have yielded similar results. Presence of attenuation and background activity does not affect the accuracy of the dSPECT reconstructions. In all situations investigated satisfactory dynamic images were produced. A preliminary normal volunteer study measuring renal function was performed. The reconstructed dynamic images may be presented as a three-dimensional movie showing movement of the tracer through the kidneys and the measurement of the regional renal function can be performed. The time–activity curves determined from this dSPECT data are very similar to those obtained from dynamic planar scans.

1. Introduction

The ability to obtain functional information from the living human body has powerful implications both in clinical practice and in research. SPECT (single photon emission computed tomography) and PET (positron emission tomography) are recognized as imaging techniques best suited to investigate organ function since they image, in three dimensions, the bio-distribution of radiolabelled pharmaceuticals within the body. At present, due to the time required for data collection, SPECT imaging is used only to study stationary distributions of tracers. Physiological processes are, however, dynamic with the distribution of biological molecules changing over time. The rate of such a change often contains information which might be useful in assessing disease (Hudon *et al* 1988, Nellis *et al* 1992).

¶ Address for correspondence: Medical Imaging Research Group, Division of Nuclear Medicine, Vancouver Hospital and Health Sciences Centre, 855 West 12th Avenue, Vancouver, BC, V5Z 1M9, Canada. Webpage: `http://kepler.physics.ubc.ca/~mirg`

In a functional dynamic study, a sequence of images is typically acquired, where each image is assumed to represent the spatial distribution of the tracer of interest at some particular moment in time. These images are then used to obtain estimates of kinetic parameters in the investigated processes. The majority of clinical dynamic studies are performed using planar imaging methods (Hudon *et al* 1988, van Eenige *et al* 1987, Tillisch *et al* 1986, Murray *et al* 1994) which lack both 3D spatial resolution and attenuation correction. In order to perform an artefact-free dynamic tomographic study while still using standard reconstruction methods, all projections for each image should be acquired simultaneously. This is possible only with PET (Phelps *et al* 1986, Mazoyer *et al* 1986) or ring SPECT cameras (Mickey *et al* 1984, Lassen and Sperling 1994). In the case of rotating-camera SPECT systems, the projections required for each single image are taken at different times, therefore, in the dynamic case, they represent different distributions of the tracer. Images reconstructed from these *inconsistent* projections contain artefacts, which may lead to errors in diagnosis (Limber *et al* 1995, O'Connor and Cho 1992, Links *et al* 1991).

Multidetector SPECT systems have a higher sensitivity than single-camera systems and are able to collect complete data sets more quickly with the same statistics. This capability has been exploited to improve the performance of conventional dynamic imaging techniques in the case of myocardial perfusion studies (Nakajima *et al* 1991, Smith and Gullberg 1994, Smith *et al* 1994). In dynamic imaging the camera must rotate fast enough for it to be able to be assumed that there is no activity change in the object during the collection of the data for each separate image. However, 'fast rotation' acquisitions (a scan as short as 10 s for a total rotation time was used by Smith *et al* (1994)) result in images which suffer from poor statistics and high noise. Further, the equipment used in these studies is highly specialized and few cameras can perform multiple, fast rotations.

An alternative approach is to estimate kinetic parameters directly from the projection data, without image reconstruction. This method, initially developed for PET (Carson and Lange 1985), has been subsequently applied to SPECT (Limber *et al* 1995, Chiao *et al* 1994, Zeng and Gullberg 1995, Reutter *et al* 1998, Maltz *et al* 1998). Most such approaches, however, still require multiple camera rotations and/or make assumptions regarding the underlying kinetic model of the investigated processes.

The focus of our research has been different. Our objective has been to develop a reconstruction technique which would not suffer from the poor statistics inherent in the fast rotation method and which could be used with readily available equipment.

Our dynamic SPECT method (referred to as dSPECT) provides for the estimation of kinetic parameters from studies performed using just a single rotation of a standard (single-, dual- or triple-head) SPECT camera. Although initially (Limber *et al* 1995) a dual-exponential model for the dynamic activity change was assumed, this restriction has since been removed and now a more general type of time behaviour is permitted (Maeght *et al* 1999, Farncombe *et al* 1999a, b, Bauschke *et al* 1999). The primary feature of dSPECT is that it is based on a mathematical method which processes all the dynamic projection data simultaneously instead of reconstructing a series of static images individually. The method makes use of the temporal information already present in the SPECT projection data when they are collected using standard clinical protocols; therefore no change to the acquisition protocol is required. The method reconstructs each dixel (dynamic voxel) independently and makes no assumption about the location of the dynamic areas. Each dixel can display dynamic behaviour different from that of its neighbours. As a result a time series of 3D images is created, each image corresponding to the distribution of activity at the time when one of the projections was acquired.

In this paper we present the results of a comprehensive study of the performance of the method for the cases when the analysed activity in the object is only decreasing or is

only increasing. Although considering this type of activity change may seem restrictive as compared with, for example, the increase–decrease which would arise in a washin–washout situation, the method has several potential clinical applications. Examples are in studies of renal washout for kidney transplant patients (after the washin phase is finished), in the assessment of myocardial viability using ^{123}I labelled fatty acids, and for the removal of reconstruction artefacts which arise from the fast filling bladder in SPECT bone scans of the pelvis. The situations with monotonic decrease or increase of activity allow us to use a different version of the reconstruction software, a version which is simpler, much faster and hopefully even more accurate than that used in the more general case. Our objective here is to investigate this particular situation. The analysis of the performance of dSPECT for the washin–washout case has been presented elsewhere (Farncombe *et al* 1999b).

As mentioned, the dSPECT method does not make assumptions about the location of the dynamic regions. However, for the general case of increasing–decreasing activity, it requires prior knowledge of the time frame where the activity peaks in each particular voxel of the imaged object and the method to determine this 'peak frame' has been developed and is described by Farncombe *et al* (1999b). This general case is more complicated than the one analysed in this work and involves two additional reconstruction steps which may influence the performance of the method as well as the accuracy of the results. The general approach will also need to be applied in situations where some voxels display decrease and others increase of activity unless the exact position of these voxels can be identified *a priori* (very unrealistic clinically) in which case the simpler method (the one described here) could be used.

Clinical validation of any new imaging method is always difficult but the problem for dSPECT is further compounded by the fact that dynamic SPECT studies are not routinely performed. The dSPECT approach is somewhat contraintuitive in that 4D dynamic images are reconstructed from data acquired in a standard manner often thought only to be applicable to 3D reconstructions of static situations. The objective of this work has thus been to investigate the method under several different imaging conditions and for different dynamic situations using simulations and phantom data (where 'the truth' is known) in order to assess its accuracy and gain the level of confidence which would be necessary before clinical tests begin. An example of a clinical study is also provided.

2. Methods

2.1. dSPECT reconstruction

The dSPECT approach relies on the fact that the data acquired during a regular SPECT scan contain more information than is normally used in the reconstruction of a static image. Each projection, as it is acquired, corresponds to a particular distribution of activity in the object at a given point in time. This additional temporal information is used to reconstruct a series of dynamic images where each image corresponds to the activity distribution at the time when the projection was acquired. Only a limited set of assumptions related to the behaviour of the activity change is made. The dynamic images are obtained iteratively by solving a shape-constrained linear least squares problem:

$$\text{minimize } f(x) = \sum_{j,k} \sigma_{jk}^{-2} \left(\sum_i a_{ijk} x_{ik} - d_{jk} \right)^2 \tag{1}$$

$$\text{subject to } x_{i1} \geqslant x_{i2} \geqslant \cdots \geqslant x_{in} \geqslant 0 \tag{2}$$

$$\text{or} \qquad 0 \leqslant x_{i1} \leqslant x_{i2} \leqslant \cdots \leqslant x_{in} \tag{3}$$

$$\text{or} \qquad 0 \leqslant x_{i1} \leqslant \cdots \leqslant x_{ip} \geqslant \cdots \geqslant x_{in} \geqslant 0 \tag{4}$$

Figure 1. Two dynamic phantoms used in simulation studies. Phantom (*a*) consists of a ring with four dynamic segments with different decay constants. The second phantom (*b*) is a model of a human thorax with stationary activity containing a heart model with two different dynamic sections. Section 1 (46 pixels, left) was modelled with a monoexponential, and section 2 (91 pixels, right) with a dual-exponential washout. Presented images correspond to distribution of activity in each phantom at 5 min after the beginning of data acquisition. Figure (*c*) shows the attenuation map used for the second phantom and models a non-homogeneous density distribution in the thorax region.

where x_{ik} corresponds to the activity in ith object voxel at time k, σ_{jk}^{-2} is a weighting factor determined from the variance of the projection bin contents d_{jk}, and a_{ijk} is a geometrical weighting factor based upon camera geometry and photon transport. Details of the reconstruction method have been reported elsewhere (Maeght *et al* 1999, Farncombe *et al* 1999a, b). Constraints (2) and (3) correspond to cases with decreasing-only and increasing-only activity changes, while constraint (4) includes both increase of activity up to the point x_{ip} and then decrease.

As already mentioned we discuss here only cases (2) and (3), case (4) being analysed in Farncombe *et al* (1999b). The reconstruction procedure for these two cases is quite different from that required for the last one since there is no need to seek the peak position, therefore a simpler approach can be used (Farncombe *et al* 1999a, b). The maximum activity in each dixel is known to be in the first or in the last time frame. In all reconstructions presented in this paper the minimization was performed using a constrained least squares method (C-LS).

2.2. Attenuation correction

As the camera rotates around the investigated object, changes in the levels of recorded activity which are due to dynamic processes cannot be distinguished from similar effects caused by attenuation. Therefore, as an integral part of the dSPECT reconstruction process, accurate attenuation correction must be performed. In simulations with an attenuating thorax phantom, the system matrices used in dSPECT reconstructions were modified to include information about the distribution of the attenuating material in the phantom. For the experimental phantom and patient studies we have used attenuation maps determined from transmission scans performed simultaneously with the dynamic acquisitions. The attenuation coefficients were incorporated in the dSPECT reconstruction process in the factors a_{ijk}. Scatter and collimator blurring corrections were not included in this study.

2.3. Simulation studies

Two different dynamic phantoms were used in our simulation studies (see figure 1). Since the dSPECT method reconstructs each slice individually, both phantoms were generated in 2D only.

For the first series of simulations an analytical ring, divided into four equally spaced segments, was simulated. Each segment initially contained the same activity concentration,

Table 1. Initial activities and half-lives $T_{1/2}$ (in minutes) of the dynamic activity changes used in ring phantom simulations with single- and dual-exponential models. The initial activities are quoted in relative units. For further explanations see text.

| Phantom | Segment | Mono-exponential | | Dual-exponential | | | |
		A_i	$T_{1/2}^{\nu}$	A_i	$T_{1/2}^{\nu}$	B_i	$T_{1/2}^{\eta}$
Ring phantom	1	1	2	1	2	1	20
	2	1	4	1	4	1	20
	3	1	8	1	8	1	20
	4	1	16	1	16	1	20

but exhibited different dynamic behaviours. Several tests were performed assuming mono- or dual-exponential washout. Since the objective of this study was to test the performance of the reconstruction method for different acquisition geometries, the attenuation effect was not modelled at this stage.

A second set of simulations was designed to test the performance of the method when both attenuation and noise were present in the data. In this case, the phantom consisted of a pixelized U-shaped 'heart' model composed of two dynamic regions with different dynamic behaviour. The heart was surrounded by an inhomogeneous attenuating thorax model consisting of soft tissue (with attenuation coefficient equal to $\mu = 0.15$ cm^{-1}), two lungs ($\mu = 0.04$ cm^{-1}) and a spinal column ($\mu = 0.22$ cm^{-1}). The overall size of the phantom was an ellipse with major and minor axes equal to 30 cm and 25 cm, which corresponded to areas of 137 pixels for the heart (46 pixels in section 1 and 91 pixels in section 2), 24 pixels for the spine, 208 pixels for the total of both lungs (104 each lung) and 1175 pixels for the soft tissue of the thorax when imaged with a pixel size of 6.25 mm.

The activity change $x_i(t)$ in each of the dynamic segments for both simulated phantoms can be described by the formula:

$$x_i(t) = A_i e^{-\nu_i t} + B_i e^{-\eta_i t} \tag{5}$$

with two situations modelled as: (a) a monoexponential where the washout function corresponded to $A_i > 0$, $B_i = 0$, and (b) a dual-exponential with the washout $A_i = B_i > 0$. Table 1 summarizes the parameters used in different simulations for the ring phantom. Half-lives $T_{1/2}^{\nu}$ and $T_{1/2}^{\eta}$ quoted in this table correspond to the dynamic decay constants ν and η respectively, with $T_{1/2}^{\nu} = \ln 2/\nu$ and $T_{1/2}^{\eta} = \ln 2/\eta$. The heart model was simulated with section 1 following a monoexponential, and section 2 a dual-exponential washout (see table 2). In the case of the ring model only relative values of activity were used, but for the heart simulations the activity values reflected the noise levels which were modelled in the data.

Three levels of thorax static background activity were investigated: (a) no background activity, (b) medium background activity, where soft tissue activity was equal to the half of the initial heart activity, and (c) high background activity, with soft tissue, lung and spine activity concentrations equal to 0.06 MBq per pixel. This last case simulated an extreme situation of high background where, at the initial moment, the activity concentration in the heart was equal to the concentration in the surrounding tissue. Table 2 presents the values of the initial activity and activity concentration in each of the two sections of the heart and each organ as used in these simulations. Poisson noise which was subsequently added to the projection data was consistent with these levels of activity.

For each simulated phantom, six different acquisition methods were modelled, corresponding to three different head configurations and camera rotation angles creating in total 18 data sets. The summary of these tests is presented in table 3. In each case, the total

Table 2. Initial activities, A_i (in MBq), and corresponding activity concentrations a_i (in MBq cm^{-2}) used in the simulations of the heart phantom. Study (a) corresponds to no background activity, while studies (b) and (c) are medium and high background respectively. For further explanation see the text.

| | Dynamic heart | | | | | | | Static | | | | | |
| | Section 1, 46 pixels | | | Section 2, 91 pixels | | | | Lungs, 208 pixels | | Spine, 24 pixels | | Body, 1175 pixels | |
	A_i	a_i	$T_{1/2}^{\nu}$	A_i	a_i	$T_{1/2}^{\nu}$	$T_{1/2}^{\eta}$	A_L	a_L	A_S	a_S	A_B	a_B
Study (a)	6	0.33	2	6	0.17	2	10	0	0	0	0	0	0
Study (b)	6	0.33	2	6	0.17	2	10	0.4	0.005	0.4	0.04	4	0.009
Study (c)	6	0.33	2	6	0.17	2	10	12	0.15	1.4	0.15	68	0.15

Table 3. Acquisition conditions (head configuration, camera rotation angle, number of projections per head and the angle per projection) used in simulations. For further explanations see the text.

| | Camera configuration | | Acquisition angle (per head) | Number of projections (per head) | Angle per view |
Acquisition	Number of heads	Relative position			
A	1	n/a	180°	64	2.8°
B	2	180°	180°	32	5.6°
C	2	90°	90°	32	2.8°
D	2	90°	180°	64	2.8°
E	3	120°	120°	30	4.0°
F	3	120°	180°	60	3.0°

n/a = not applicable.

acquisition time was equal to 20 min with projection data acquired into 64 camera bins. The number of projections acquired by each head was set so that the total number of projections was equal to 64 per 180° camera rotation. Exceptions were made in cases of the dual-head camera with heads at 180° and for the triple-head camera where this number was 32 per head and 30 projections per 120° rotation (which is equivalent to 45 projections over 180° rotation) and 60 projections for 180° rotation.

2.4. Dynamic phantom experiments

Following computer simulations, experimental studies were performed using our dynamic heart-in-thorax phantom (Celler *et al* 1997) under a variety of configurations.

The phantom consists of two independent parts: (a) a dynamic heart model with the possibility of mounting up to five containers (small bottles) modelling heart defects inside it and (b) a non-uniform thorax model with lung and spinal cord inserts. Only heart model (a) was used in the present studies. The design of the phantom is based on the fact that the washout of a tracer by dilution follows a linear first-order differential equation, the same type of equation as is used, for example, to model time–activity distribution in myocardial viability studies (van Eenige *et al* 1987). Initially, each of the dynamic sections of the phantom is preloaded with activity and the flow of water at a uniform rate produces activity dilution which mimics metabolic activity changes. Uniform activity distribution in each dynamic section is achieved by using a mixing propeller (installed inside each container) and a dedicated electric infusion pump maintains constant water flow.

Table 4. Initial activities and half-lives $T_{1/2}$ (in minutes) of the dynamic activity changes used in phantom experiments together with the corresponding values obtained from dSPECT reconstructions. The initial activities (in kcounts s^{-1}) could be determined only for experiments with no attenuation. For further explanations see text.

	Container	Simulated values		Reconstruction results	
		A_i	$T_{1/2}^{\nu}$	A_i	$T_{1/2}^{\nu}$
Experiment I,	1	2.5	2.0	2.2	2.0
method A	2	7.4	3.3	7.3	3.2
(bottles in air)	3	1.3	4.1	1.6	3.2
(no atten.)	4	6.0	5.5	6.3	5.3
Experiment II,	1	2.3	2.1	2.1	2.2
method F	2	7.0	3.6	7.2	3.3
(bottles in air)	3	1.2	4.6	1.4	4.0
(no atten.)	4	5.6	6.1	5.9	5.7
Experiment III,	1	4.5	2	4.8	2.0
method C	2	3.9	4	3.6	4.2
(bottles in air)	3	3.7	6	3.5	6.0
(no atten.)	4	2.9	8.5	3.2	8.6
	5	2.5	18	3.1	21.5
Experiment IV,	1	n/a	2.0	n/a	2.7
method C	2	n/a	3.0	n/a	4.2
(bottles in water +	3	n/a	6.0	n/a	6.8
water bags, with atten.)	4	n/a	Static	n/a	12.8

n/a = not applicable.

Four different dynamic phantom experiments have been performed using three different camera geometries, resulting in four different sets of dynamic data (see table 4). In the first experiment (I), four dynamic containers (17 ml bottles) were used with a triple-head camera performing an acquisition with a 180° rotation per head. In this experiment the data from each head were used individually (table 3, method A). The same experimental set-up was used in the second experiment (II). This time, however, the data from all three heads were used together, each head performing an entire 180° rotation (table 3, method F). The containers were placed in air (no attenuation) and a Siemens MS3 camera was used in both cases.

A third study (III) was performed using a dual-head Siemens Ecam system with heads positioned at 90° with a rotation of 90° per head (table 3, method C). The same dynamic phantom was used, but this time with five (instead of four) dynamic containers. The last experiment (IV) was performed, again using four containers and following method C, but this time including the effects of attenuation. All four bottles were placed in the heart container filled with water and, additionally, three 1 litre water bags were attached around its circumference. Attenuation maps of the phantom were reconstructed from the transmission scan acquired simultaneously with the emission study using a *Profile* multiple line source system (Celler *et al* 1998).

Table 4 summarizes the experimental conditions used in our phantom studies. In most cases the initial activity injected into in each container was approximately 37 MBq. The total acquisition time in all experiments was about 12 min (10 s per projection) with 64 projections acquired per head. The matrix size was 64×64 with zoom 1.5 for the MS3 camera (pixel size 0.36 cm) and 128×128 without zoom for the Ecam (pixel size 0.48 cm). In order to reduce the matrix size used in reconstruction, the outside boundaries of each projection matrix of the

Ecam data were truncated into a 64×128 size and every two projections in the sequence were summed into one resulting in a 64 projection data set (32 per head). The $T_{1/2}$ of the activity washout were determined by the speed of the infusion pump. The accuracy of this procedure was found to be of the order of 1–2% (Celler *et al* 1997).

2.5. Human studies

A dynamic ^{99m}Tc MAG3 (370 MBq) renal study was performed for a normal human subject (prone position) using the Ecam dual-head camera with heads at $90°$ each rotating over $90°$ (method C) (informed consent from the normal volunteer has been obtained). This first human study was done solely in order to verify that the dSPECT reconstruction method can deal with real patient data. Similar to the phantom experiment, transmission data using the *Profile* transmission system were acquired simultaneously with the dynamic emission data in order to determine patient-specific attenuation maps. A 12 min dynamic tomographic acquisition was started 2 min after the injection to cover only the washout part of the study. The projection matrix size was 128×128 with a total of 128 projections acquired (64 per head).

Additionally, a dynamic planar scan was performed several hours prior to the SPECT scan in order to determine approximate renal kinetics. The performance of the dSPECT reconstruction was assessed by comparison with this planar scan. This was done by reprojecting the reconstructed dSPECT data into planar images.

2.6. Data analysis methods

Each dSPECT reconstruction results in the creation of a dynamic series of transaxial images corresponding to the times of each projection. The spatial accuracy of these reconstructions was assessed visually by comparison with the true images as used in the simulation cases and with the known location of the containers in the phantom experiments.

In order to estimate the quantitative accuracy of dSPECT reconstructions, the true kinetic parameters were compared with the values obtained from the reconstructed images. The $T_{1/2}$ related to the dynamic behaviour of the activity in each segment was determined using time–activity curves obtained for different 2D regions of interest (ROIs). In simulations, these ROIs corresponded to the area of each dynamic segment. For phantom experiments a separate ROI was drawn for each container. For the computer simulations, the reconstructed initial activity in each segment and the corresponding washout half-life were compared with the true values. In the phantom experiments, the reconstructed $T_{1/2}$ was compared with the preset value. For each bottle the initial activity (count rate) obtained from the reconstruction was compared with the experimental value of the initial activity as determined from the total number of counts present in an appropriate ROI drawn on the first projection. This method, however, can only be used in experiments without attenuation and where there is no overlap of the dynamic containers in the projections.

The same quantitative analysis was not possible for the patient study, however, as the true values of the initial activity and of kinetic parameters were not known. In this case, only visual inspection and comparison with the planar dynamic images was performed.

3. Results and discussion

3.1. Simulation studies

Results of reconstructions of the ring object acquired using different system configurations for mono- and dual-exponential decay are similar. Therefore, only the more complex situation
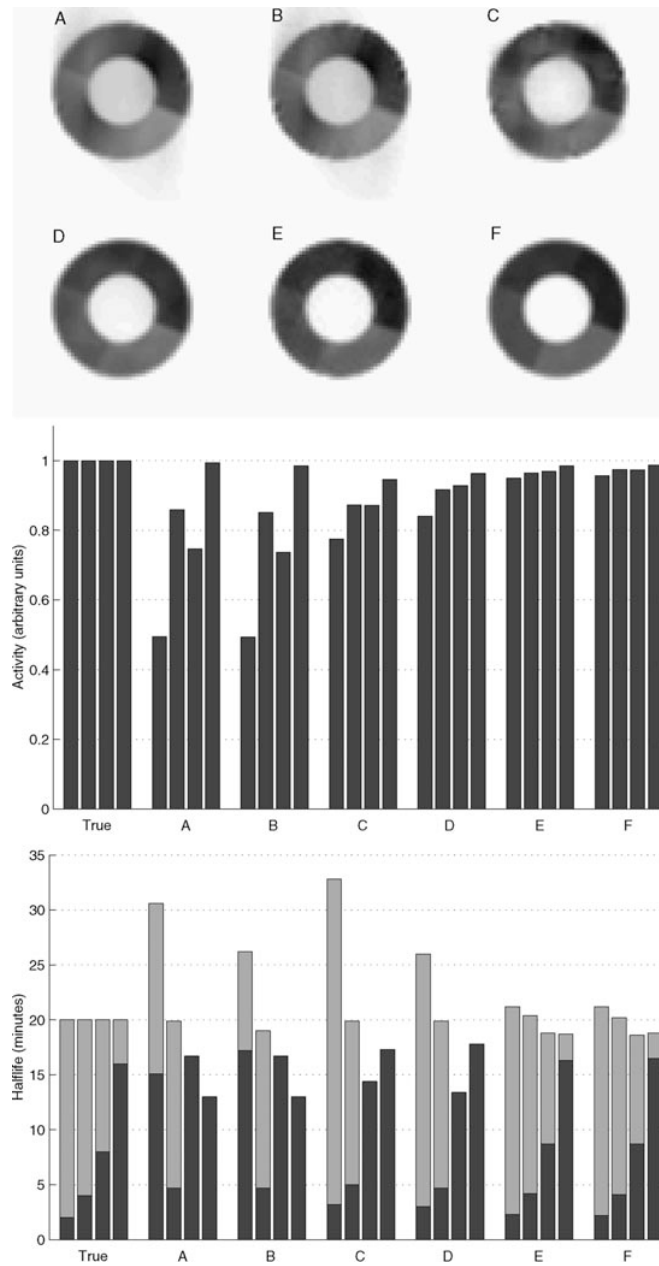
Figure 2. Dynamic images (top part) of a ring phantom reconstructed from the data simulated with dual-exponential activity washout and acquired using six different methods as presented in table 3. Only one image, corresponding to the activity distribution at 5 min, is shown from each series. The true distribution of activity is displayed in figure 1(*a*). The lower part compares the true and reconstructed initial activities (middle) and half-life values (bottom). For the analysis of half-lives, the values of the grey and black bars correspond to the long and the short component of the dual-exponential function respectively.

of dual-exponential washout is shown in figure 2 with only one image from each of the reconstructed series. This image corresponds to the activity distribution in the phantom 5 min after the beginning of acquisition.

For all investigated cases the shape of the object reconstructs well, with only small streaks visible outside the ring. As expected, the best reconstructions are obtained from a triple-head camera (figure 2, E and F). This is due to the fact that in this configuration three independent views of the same object are acquired from different angles at the same moment in time. A dual-head camera with heads at $90°$ (figure 2, C and D) produces very comparable results. The images obtained from the single-head system and a system with two heads positioned at $180°$ are the worst and display substantial streak artefacts (figure 2, A and B). These artefacts, which in each image occur in the direction towards the position of the camera at a given time frame, are marked in the first few images in the series and gradually disappear in later images. The quality of images obtained from acquisitions following methods A and B is also very similar, confirming that where there is no attenuation, a second camera head positioned opposite to the first one does not improve the reconstruction since it does not provide us with any additional meaningful data but rather only improves statistics.

The same conclusions can be drawn from analysis of the numerical results from those studies summarized in the lower part of figure 2. The length of the bars represents the values of the true and the reconstructed activity (middle part) and corresponding $T_{1/2}$ (bottom part) for each segment in the phantom and each acquisition method. It is important to remember, while considering multiple exponential data, that several different sets of exponential functions can often be fitted almost equally well to the same experimental data. Some discrepancies between the true $T_{1/2}$ values and the values obtained from the dual-exponential fit to the reconstructed data can be due to this effect.

The images obtained from simulations of the heart model in the attenuating thorax phantom with medium activity level are presented in figure 3. The corresponding numerical values are summarized in the lower part of this figure. The same pattern as in the previous case can be seen here when analysing the accuracy of reconstructions of the initial activity and $T_{1/2}$. The overall errors amount to about 10% for the triple-head camera and are slightly larger for the dual-head system. Reconstructions from the single- and $180°$ dual-head cameras gave the highest errors.

In summary, the accuracy of reconstructions for the triple-head system for most segments is better than 90% with only a small difference between the results obtained from $120°$ and $180°$ camera rotation. The quality and accuracy of reconstruction degrades gradually when moving to the less complex camera systems and smaller rotation angles. The accuracy obtained from a dual-head $90°$ system performing $180°$ rotation of each head is in the range of 80–90% while single-head accuracy is only about 50%. All systems have problems reconstructing dual-exponential decay with two similar values of $T_{1/2}$, although the error in the case of a triple-head camera is the smallest.

An important conclusion from these last studies is that the dSPECT reconstruction method performs equally well with and without the attenuation effect. In some cases the accuracy of reconstructions improved when attenuation was included in simulations, as in this case the data acquired by detectors at different angles contains additional and complementary information about the activity in the object (compare, for example figures 2B and 3B).

Finally, figure 4 compares the quality of reconstructed dynamic images for the distribution of activity at 5 min after the beginning of acquisition for the thorax phantom with (a) no background activity, (b) medium background and (c) high background activity. Only reconstructions of the data acquired using methods D and F are shown since they produced the best images. Corresponding graphs in figure 4 analyse the accuracy of the reconstructed
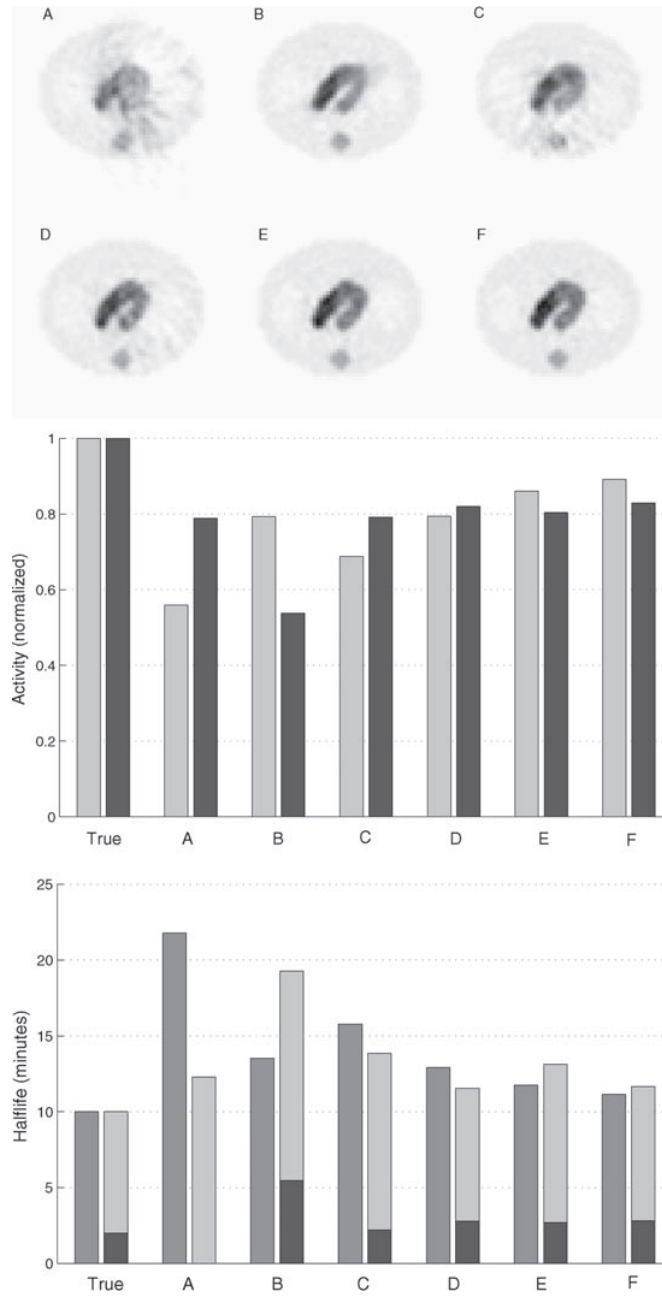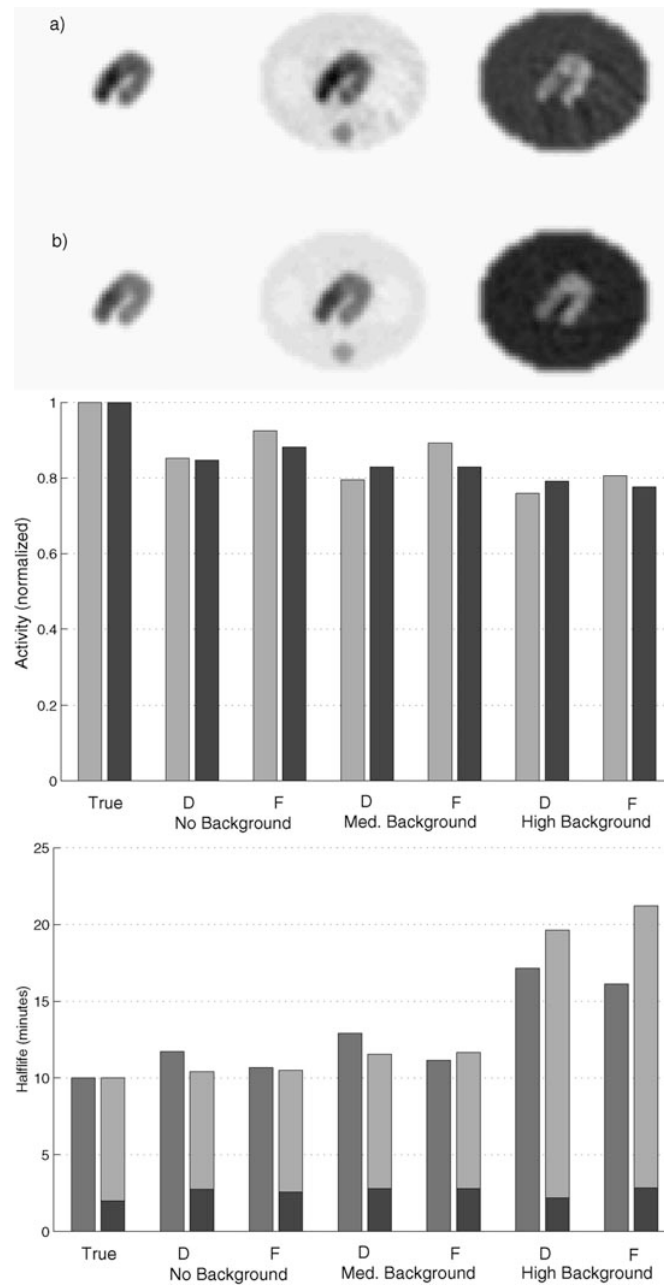
Figure 3. Reconstructions of the heart model in the attenuating thorax with medium background activity for the six acquisition methods (top). Only one image, corresponding to the activity distribution at 5 min, is presented from each series. The true distribution of activity is shown in figure 1(*b*). The figure in the middle presents the initial activity values, and the bottom part depicts washout half-lives. For the analysis of half-lives the values of the dark grey, light grey and black bars correspond to the monoexponential and the long and short components of the dual-exponential function respectively.
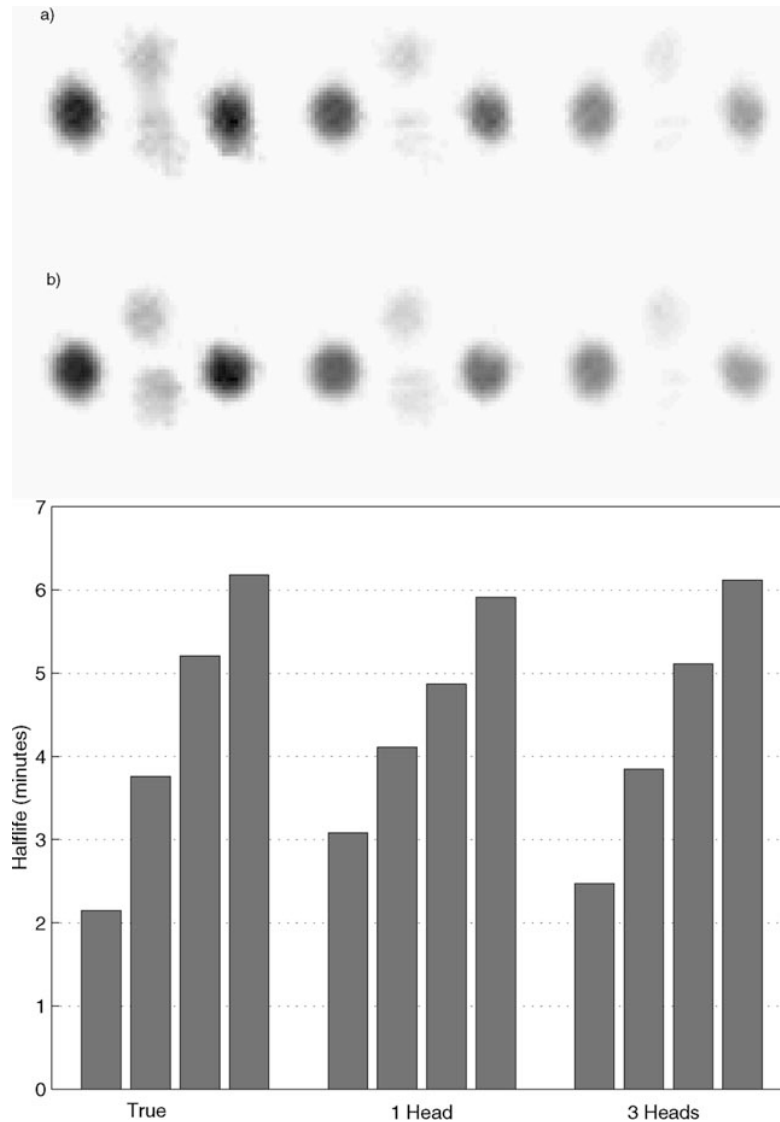
Figure 4. Reconstructions of the heart model in the attenuating thorax medium for three different levels of background activity (top part). Only one image, corresponding to the activity distribution at 5 min, is presented from each series. The reconstructions shown correspond to the data acquired with (*a*) dual-head 90° camera, with each head performing 180° rotation (acquisition type D), and (*b*) triple-head 120° camera with 180° rotation per head (acquisition type F). The middle figure presents the initial activity values and the bottom figure shows washout half-lives. For the analysis of half-lives the values of the dark grey, light grey and black bars correspond to the monoexponential and the long and short components of the dual-exponential function respectively.

Figure 5. Reconstructed images of the four containers of the dynamic phantom. Images represent the activity distribution at 3 min, 6 min and 9 min after the beginning of the data acquisition. The data were acquired with a triple-head camera. Figures presented at the top (*a*) were reconstructed from a single-head 180° rotation (method A, experiment I); part (*b*) shows the same reconstruction acquired with all three heads rotating each over 180° (method F, experiment II). Reconstructed half-lives are compared to the true values in the bottom part of the figure.

activities and the $T_{1/2}$s. In all three cases the error in activity reconstruction is below 20%. A similar level of agreement is obtained for $T_{1/2}$ for cases (a) and (b). For case (c), although the fast $T_{1/2}$ reconstructs well, the accuracy of the reconstruction of the slower component is less accurate. Nevertheless, even in this extreme case of high activity level in the tissue surrounding the dynamic organ, the boundaries are clearly visible and the fast $T_{1/2}$ is well identified.
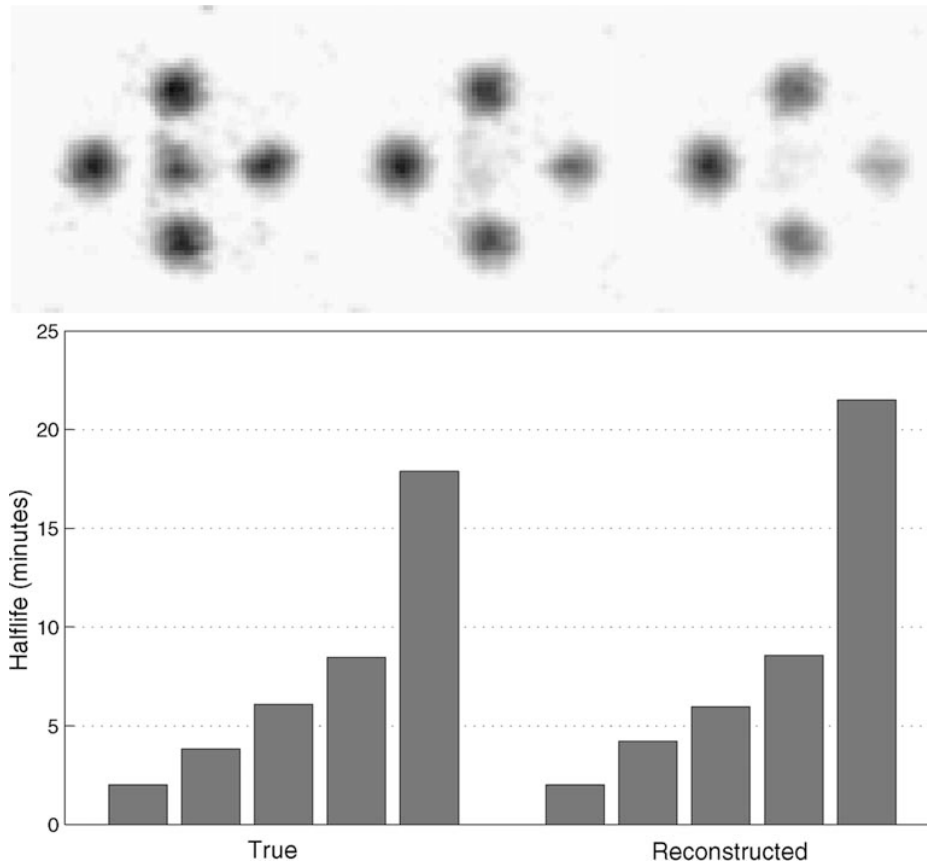
Figure 6. Reconstructed images (top) of the five containers of the dynamic phantom (experiment III). Images represent the activity distribution at 3 min, 6 min and 9 min after the beginning of the data acquisition. Data were acquired with a dual-head camera with heads at 90° rotating through 90° (method C). Reconstructed half-lives are compared with the true values in the bottom part of the figure.

3.2. Dynamic phantom experiments

Reconstructions of the experimental phantom data yield very similar results to those obtained through simulations (see figures 5, 6 and 7). That is, visual inspection of these images shows that the reconstructions of the data acquired with three heads outperform those acquired with one- and two-head camera systems. However, these differences are small and the half-life reconstructions (see table 4 for a summary of the results) for dual-head acquisitions are still accurate to within 90%. Similarly, the experiments involving the phantom with attenuation confirmed our earlier findings that the dSPECT method performs well in this situation provided that the attenuation maps are included in the reconstructions. It should be noted at this point that the experiment with the dual-head system did not use the optimized acquisition protocol as was determined from computer simulations. It is hoped that the upgrades to the camera which are pending will enable optimal protocols to be used and this will result in increased accuracy.
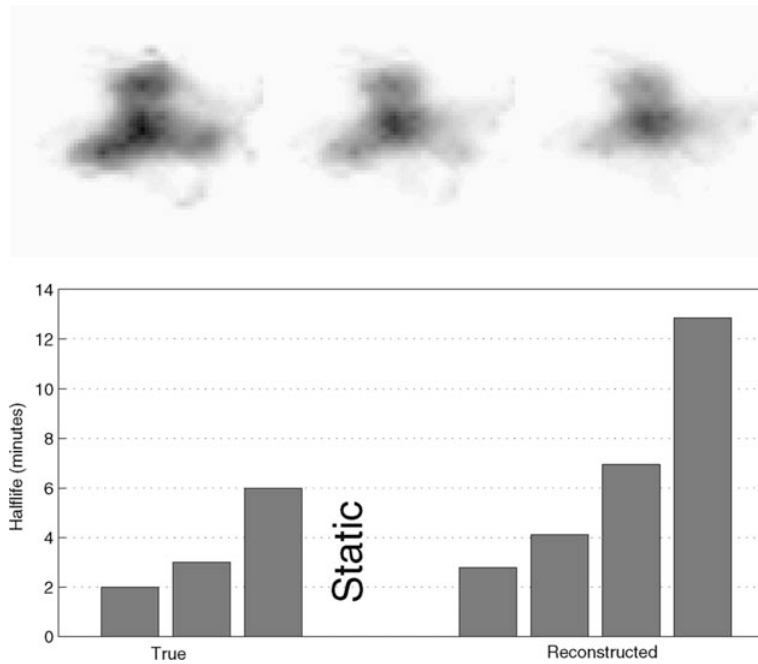
Figure 7. Reconstructed images of the four containers of the dynamic phantom with attenuation (experiment IV). Images represent the activity distribution at 3 min, 6 min and 9 min after the beginning of data acquisition. Data were acquired with a dual-head camera with heads at 90° rotating through 90° (method C). Reconstructed half-lives are compared with the true values in the bottom part of the figure.

3.3. Human studies

Since dynamic SPECT data of the human kidneys are not available and true changes in activity distribution are not known, the dSPECT results were compared only with dynamic planar studies. Twenty seven transaxial slices of the renal glomerular filtration rate (GFR) study reconstructed by the dSPECT method were reprojected to allow for such a comparison. These reprojected dSPECT images show increased contrast due to the inherent attenuation correction used in these studies. Figure 8 compares these two planar images and shows one transaxial slice from this dSPECT reconstruction. However, these results can be much better appreciated by playing a dynamic 4D movie of the reconstructed human kidney which can be found on our webpage (http://www.physics.ubc.ca/∼mirg/dyn_visual.html). The time–activity curves from region-of-interest analysis of reprojected dSPECT data shows similarity to planar dynamic data, although at this point it is not known if the observed differences are a result of including the attenuation correction, differences in renal GFR, or are due to the reconstruction process used.

4. Comparison with fast camera rotation protocol

Since our results indicate that the dSPECT method performs best when used with multiple-head cameras, one might ask what advantages, if any, the dSPECT approach has over fast rotation dynamic SPECT acquisitions.
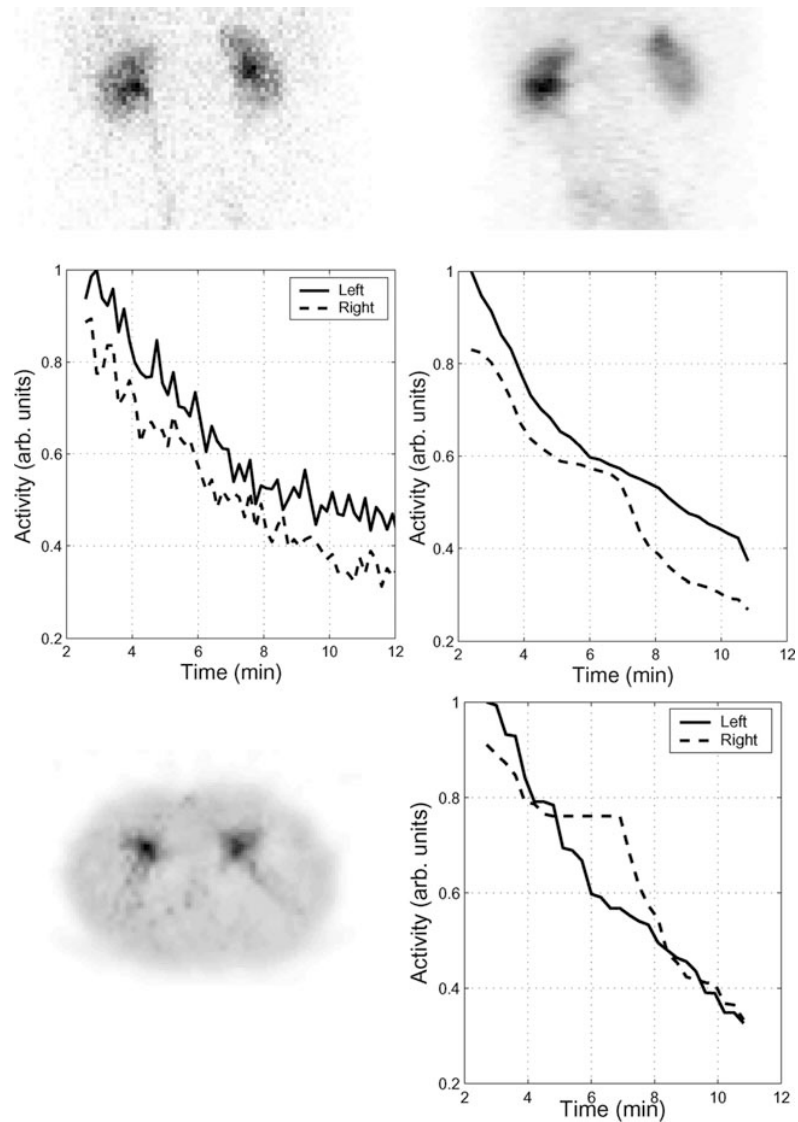
Figure 8. Dynamic planar image (top left) and an image reprojected from a dSPECT scan (top right) of an MAG3 renal study of a normal subject. Only the decaying part of the renogram was analysed in this study. The graphs in the middle of the figure show time–activity curves (TAC) obtained from the ROIs drawn on the left (full line) and right kidney (broken line), respectively. The bottom part presents one transaxial dSPECT slice (patient in prone position) and the corresponding time-activity curves (TAC). The TACs were normalized to the planar studies.

Firstly, the acquisition process of dSPECT is much simpler and much easier to implement clinically. Data sets for dSPECT are the same as those used in standard static SPECT studies their size being of the order of only a few megabytes, whereas projection data in fast rotation studies are hundreds of megabytes in size. Additionally, it should be noted that most camera

systems are not able to perform fast rotations, which seriously restricts the use of the fast rotation method, whereas the dSPECT method performs well (accuracy to within 80%) with the data acquired using a standard acquisition protocol with any standard dual- or triple-head SPECT system.

Reconstruction of a series of 32 dSPECT time images for one transaxial slice from the data composed of 32 projections and a matrix 64×64 takes about 5 min on a Pentium II 400 MHz computer. We believe that this time can be substantially shortened as our present reconstruction program in its 'research version' runs in the MATLAB environment and is far from being optimized.

Each method results in the creation of a dynamic sequence of images which may be used in later kinetic analysis. If the total acquisition time for fast rotation SPECT and slow dSPECT acquisitions is the same, the same total number of counts will be collected in both studies. There are, however, important differences between the two approaches arising from the fact that the data are collected and used differently.

The fast rotation dynamic SPECT method uses multiple fast rotations of a triple-head camera, thus the resulting data consist of many subsets, each corresponding to one camera rotation. Each particular subset consists of several projections which are later used to reconstruct one image of the sequence corresponding to the time of the given rotation. As a consequence, each particular projection in such a study contains only a low number of counts resulting in a low signal to noise ratio (SNR). The reconstructed images reflect this low SNR, resulting in reconstruction artefacts.

In contrast, the data for a dSPECT study are acquired as one single set of projections. This complete set is used as a single unit in a dSPECT reconstruction to form an entire dynamic sequence of images. Since the total number of counts is divided in only one way (as opposed to two ways for the fast rotations), the data in a dSPECT projection contain many more counts than that in a fast rotation projection. This results in a much higher SNR in the data, which contributes to improved image quality. The dSPECT simultaneous reconstruction from the whole data set takes advantage of the fact that the images are correlated since they represent the history over time of the same object.

5. Conclusions

We report a new method of imaging changing activity distributions in three dimensions. The dSPECT method allows reconstruction of a dynamic series of 3D images from data acquired in a standard manner, that is using only a single slow rotation of the camera. Several tests using computer simulations, dynamic phantom experiments and a dSPECT and a planar human renal study have been performed. Single-, dual- and triple-head SPECT systems have been investigated for different acquisition protocols. Total acquisition times ranged from 12 min to 20 min. The objects investigated in simulations and phantom experiments contained multiple dynamic regions with decreasing activity which followed a single- or dual-exponential curve with the half-lives ranging from 2 min to 20 min. Effects on the quality and accuracy of reconstructions of including different levels of the stationary background activity, a non-homogeneous attenuating medium and statistical noise in the data, have been studied.

Our results indicate that in all investigated situations dSPECT reconstructions produce satisfactory dynamic images. The quality of images is best for triple-head acquisitions, because in this case the data contain the most information about spatial and temporal distribution of activity (three views for each time-frame). When comparing our results with true values we found that the accuracy of reconstruction of the initial activities and the $T_{1/2}$s is about 85–90%. Although dSPECT reconstructions of the data collected with a dual-head system with heads

at 90° result in slightly worse images, the accuracy remains within the 70–90% range. Images reconstructed from acquisitions with a single-head camera and a 180° dual-head system contain some streak artefacts and result in about 50% error. Including attenuation and noise in the data does not change the overall performance of the dSPECT method.

This new method has several advantages over existing dynamic imaging techniques in that it utilizes conventional SPECT hardware, uses typical SPECT acquisition protocols and maintains a high signal to noise ratio. While thus far tested primarily with activity decay consisting of mono- and dual-exponential washout, the method is general enough to deal with any form of decreasing activity change. Exponential functions were used only as examples since this type of functional behaviour is most often assumed in practice.

Some of the results we have obtained recently (not reported here) indicate that, with the incorporation of a spatial–temporal regularizer, streak artefacts seen in some reconstructions can be reduced further, resulting in even more accurate reconstructions. We are currently extending the dSPECT algorithm to deal with the more clinically relevant cases of increasing/decreasing activity (Farncombe *et al* 1999b).

In conventional SPECT protocols, it is assumed that the activity is fixed in space during the scan, that is, it does not change while the data are acquired. This is, however, an approximation and we suggest that the use of the dSPECT method in this circumstance might reduce any artefacts caused by tracer motion. The main applications of our method are, however, likely to be in imaging truly dynamic processes in order to visualize normal or altered organ function. Potentially it could be also used to account for patient motion during a SPECT scan, or for dynamic imaging with rotating PET or coincidence-mode SPECT cameras.

Although, the most interesting clinical applications of dSPECT may well be in completely new areas, some situations where the method could prove useful can be suggested even at this early stage by making use of existing tracers. These include renal clearance studies (^{99m}Tc MAG3, ^{99m}Tc DTPA), myocardial viability studies (^{123}I labelled fatty acids, ^{201}Tl, ^{99m}Tc Teboroxime), receptor studies in the brain and cerebral blood flow imaging (^{133}Xe, ^{127}Xe, ^{123}I). Another area that may potentially benefit from dSPECT studies is pharmaceutical research, where the changes in biodistribution of a new drug (labelled with radioactive isotope) can be traced in time.

Acknowledgments

References

Bauschke H H, Noll D, Celler A and Borwein J M 1999 An EM algorithm for dynamic SPECT tomography *IEEE Trans. Med. Imaging* **18** 252–61

Carson R E and Lange K 1985 The EM parametric image reconstruction algorithm *J. Am. Statist. Assoc.* **80** 20–2

Celler A, Farncombe T, Harrop R and Lyster D 1997 Dynamic heart-in-thorax phantom for functional SPECT *IEEE Trans. Nucl. Sci.* **44** 1600–5

Celler A, Sitek A, Stoub E, Hawman P, Harrop R and Lyster D 1998 Investigation of an array of multiple line sources for SPECT transmission scans: Simulation, phantom and patient studies *J. Nucl. Med.* **39** 2183–9

Chiao P C, Rogers W L, Clinthorne N H, Fessler J A and Hero A O 1994 Model-based estimation for dynamic cardiac studies using ECT *IEEE Trans. Med. Imaging* **13** 217–26

Farncombe T, Celler A, Bever C, Noll D, Maeght J and Harrop R 1999b Incorporation of organ uptake into dynamic SPECT reconstructions *IEEE Trans. Nucl. Sci.* accepted

Farncombe T, Celler A, Noll D, Maeght J and Harrop R 1999a Dynamic SPECT imaging using a single camera rotation (dSPECT) *IEEE Trans. Nucl. Sci.* **46** 1055–61

Hudon M P, Lyster D M, Jamieson W R E, Qayumi A K, Keiss M, Rosado L J, Autor A P, Sartori C, Dougan H and Van Den Broek J 1988 Efficacy of (^{123}I)-iodophenyl pentadecanoic acid (IPPA) in assessment myocardial metabolism in a model of reversible global ischemia *Eur. J. Nucl. Med.* **14** 594–9

Lassen N A and Sperling B 1994 ^{99m}Tc-bicisate reliably images CBF in chronic brain diseases but fails to show reflow hyperemia in subacute stroke: Report of a multicenter trial of 105 cases comparing ^{133}Xe and ^{99m}Tc-bicisate (ECD, Neurolite) measured by SPECT on the same day *J. Cerebral Blood Flow Metabol.* **14** (suppl 1) S44–8

Limber M N, Celler A, Barney J S, Limber M A and Borwein J M 1995 Direct reconstruction of functional parameters for dynamic SPECT *IEEE Trans. Nucl. Sci.* **42** 1249–56

Links J M, Frank T L and Becker L C 1991 Effect of differential tracer washout during SPECT acquisition *J. Nucl. Med.* **32** 2253–7

Maeght J, Noll D, Celler A and Farncombe T 1999 Methods for dynamic SPECT *Laboratoire MIP Technical Report* (http://mip.ups-tlse.fr/publi/rapp99/99.26.html)

Maltz J, Polak E and Budinger T 1998 Multistart optimisation algorithm for joint spatial and kinetic parameter estimation in dynamic ECT *1998 IEEE Medical Imaging Conf. Record* (CD ROM)

Mazoyer B M, Huesman R H, Budinger T F and Knittel B L 1986 Dynamic PET data analysis *J. Comput. Assisted Tomogr.* **10** 645–53

Mickey B, Vorstrup S, Voldby B, Lindewald H, Harmsen A and Lassen N A 1984 Serial measurement of regional cerebral blood flow in patients with SAH using ^{133}Xe inhalation and emission computerized tomography *J. Neurosurgery* **60** 916–22

Murray G L, Schad N C, Magill H L and Vander Zwaag R 1994 Myocardial viability assessment with dynamic low-dose iodine-123-phenylpentanoic acid metabolic imaging: Comparison with myocardial biopsy and reinjection SPECT thallium after myocardial infarction *J. Nucl. Med.* **35** 43S–48S

Nakajima K, Taki J, Bunko H, Matsudaira M, Muramori A, Matsunari I, Hisada K and Ichihara T 1991 Dynamic acquisition with a three-headed SPECT system: application to technetium 99m-SQ30217 myocardial imaging *J. Nucl. Med.* **32** 1273–7

Nellis S, Liedtke A and Renstrom B 1992 Fatty acid kinetics in aerobic myocardium: characteristics of tracer carbon entry and washout and influence of metabolic demand *J. Nucl. Med.* **33** 1864–74

O'Connor M K and Cho D S 1992 Rapid radiotracer washout from the heart: Effect on image quality in SPECT performed with a single-headed gamma camera system *J. Nucl. Med.* **33** 1146–51

Phelps M E, Mazziotta J C and Schelbert H (ed) 1986 *Positron Emission Tomography and Autoradiography: Principles and Applications in Brain and Heart* (New York: Raven)

Reutter B, Gullberg G and Huesman R 1998 Kinetic parameter estimation from attenuated SPECT projection measurements *IEEE Trans. Nucl. Sci.* **45** 3007–13

Smith A M and Gullberg G T 1994 Dynamic cardiac SPECT computer simulations for teboroxime kinetics *IEEE Trans. Nucl. Sci.* **41** 1626–33

Smith A M, Gullberg G T, Christian P E and Datz F L 1994 Kinetic modeling of teboroxime using dynamic SPECT imaging of a canine model *J. Nucl. Med.* **35** 484–95

Tillisch J, Brunken R, Marshall R, Schwaiger M, Mandelkern M, Phelps M and Schelbert H 1986 Reversibility of cardiac wall-motion abnormalities predicted by positron tomography *New Engl. J. Med.* **314** 884–8

van Eenige M J, Visser F C, Duwel C M B, Bezemer P D, Westera G, Karreman A J P and Roos J P 1987 Analysis of myocardial time-activity curves of ^{123}I-heptadecanoic acid. I. curve fitting *Nuklearmedizin* **26** 241–7

Zeng G L and Gullberg G T 1995 Estimating kinetic parameters directly from projection measurements *IEEE Trans. Nucl. Sci.* **42** 2339–46